Processes during Thermal Treatment

The processes discussed in this chapter include the mechanisms and temperature ranges of chemical reactions and phase transformations, which take place during the treatment of strontium aluminate raw materials as the mixture of strontium carbonate and alumina. Fig.1 shows the equilibrium phase composition during the preparation of calcium (a), strontium (b) and barium aluminate clinker (c). These systems show many similarities, therefore alumina react with carbonate in the molar ratio close to one. Therefore, is interesting to compare the changes of equilibrium composition which take place with increasing temperature for clinkers and pure carbonates (d).
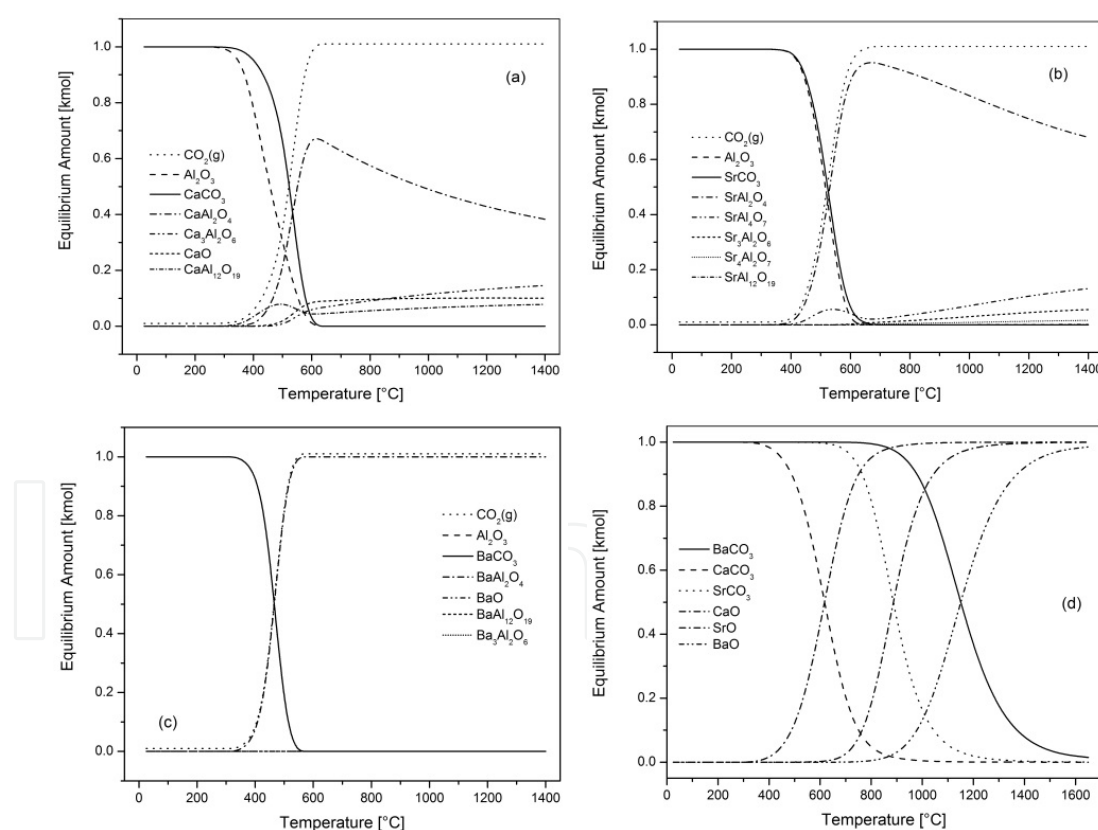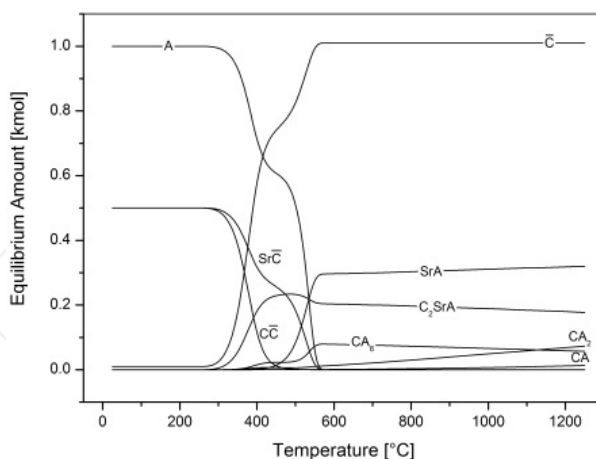

Figure 1. Calculated equilibrium composition during the thermal treatment of calcium (a), strontium (b) and barium aluminate cement (c) and thermal decomposition of pure carbonates (d).

It can be seen that strontium dialuminate phase should be formed first via the reaction of alumina with strontium oxide after the thermal decomposition of strontium carbonate. The maximum amount of strontium dialuminate occurs at the temperature of 540 °C. The amount of $SrO \bullet 2Al_2O_3$ phase decreases with increasing temperature and formed amount of strontium aluminate. This behaviour is in agreement with experimental results (Chapter 4.3), but the temperature of the process is lower. On the other hand, the differences between the equilibrium temperature and the temperature determined by experiment are common fact for heterogeneous systems, where the kinetic obstacles e.g. related to the nucleation of product occur. The content of strontium aluminate reaches the maximum at the temperature of 675 °C. Except for strontium hexaaluminate, the content of other phases from $SrO - Al_2O_3$ system increases with increasing temperature.

The similar behaviour can be observed for calcium aluminate cement, where higher aluminate phases (SrA_2 and SrA_6) are formed prior to calcium aluminate. On the contrary the formation of higher aluminate phases did not occur during the formation of barium aluminate. The formation of all three aluminates depends on the thermal decomposition of carbonates where the equilibrium constant of the process is not changed by the activity of formed clinker minerals. The mechanism, kinetics and thermodynamics of the process of thermal decomposition of strontium carbonate are discussed in Chapter 4.2.

The equilibrium composition in the mixture of ternary system $CaO - SrO - Al_2O_3$, which consists of $CaCO_3$, $SrCO_3$ and Al_2O_3 in the molar ratio ½ : ½ : 1 is shown in Fig.2. Increasing amount of CaO and SrO in the raw material (Fig.3) supports the formation of C_2SrA and SrA in the reaction mixture, respectively.

Figure 2. Influence of temperature on the equilibrium composition in the ternary system.

It was observed that increasing amount of glassy phase led to greenish tinge of fired clinker while the material treated to the temperature at which the glassy phase could not be formed was white. On the other hand, increasing amount of glassy phase increased the demand on milling of the clinker to strontium aluminate cement.
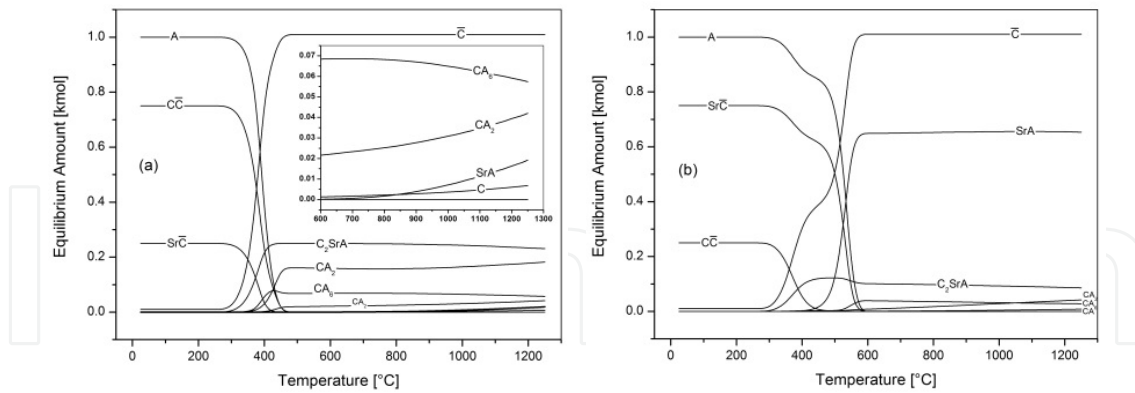
Figure 3. Temperature dependence of equilibrium composition in the systems with higher content of CaO (a) and SrO (b).

1. Thermal treatment of alumina

The α-Al$_2$O$_3$ modification of alumina can be used for the synthesis of strontium aluminate clinker. On the other hand, the most stable and well crystalline phases are also less reactive. That often means a long time synthesis which must be performed at high temperatures. Due the thermodynamic reasons, it is better to use **aluminium hydroxides** (Al(OH)$_3$ or Al$_2$O$_3\cdot$3H$_2$O), **oxyhydroxides** (AlO(OH) or Al$_2$O$_3\cdot$H$_2$O) or the **transitional alumina oxides** (Fig.4) for the preparation of strontium aluminate as the main clinker mineral for strontium aluminate cements.

Individual Al(OH)$_3$ polymorphs differ in the terms of stacking sequences of layers which are bound together by weak hydrogen bonds. The following main types of aluminium hydroxides and oxohydroxides are [325-335]:

- **Gibbsite (hydrargyllite**, Fig.5(a)) is the monoclinic γ-Al(OH)$_3$ (P2$_1$/n, a=8.684 Å, b=5.078 Å, c=9.736 Å, β=94.54°). The crystals mostly show tabular pseudohexagonal habit. The structure of gibbsite is often drawn as sheets of *hcp* layers with open packing between successive sheets. In the lateral extension of hexagonal closed packed sheets each Al^{3+}ion is coordinated by six hydroxyl (OH) groups. Each OH group is coordinated by two Al^{3+}ions with one vacant octahedral site. Six octahedra, each sharing two edges, yield [Al$_6$(OH)$_{12}$]$^{6+}$ ring. Gibbsite shows a perfect cleavage parallel to the basal plane (001). The layers are arranged in the AA-BB-AA sequence. Gibbsite was firstly described in 1820 [336,337].

- **Bayerite** (Fig.5(b)) is the monoclinic α-Al(OH)$_3$ (P2$_1$/a, a=5.0626 Å, b=8.6719 Å, c=9.4254 Å, β=90.26°). It mostly occurs in very fine fibers in radiating hemispherical aggregates and sometimes forms flaky tabular crystals with the size of about 0.1 mm. The crystal lattice of bayerite is composed of layers of hydroxyl groups similar to those in gibbsite. These layers are arranged in the AB-AB-AB sequence, so that hydroxyl groups of the third layer lie in

the depressions between hydroxyl positions of the second layer. Bayerite was firstly described in 1925 [338].

- **Boehmite** is rhombic γ-AlO(OH) (*Amam*, a=3.6936 Å, b=12.214 Å, c=2.8679 Å) which has the same structure as γ-FeO(OH). The structure of boehmite consists of double layers of oxygen octahedra partially filled with Al^{3+}cations. The stacking arrangement of the three oxygen layers is such that the double octahedral layer is in cubic closed packing. Within the double layer one can distinguish two different types of oxygen. Each oxygen atom in between the double layer is shared by four other octahedra, while oxygen atoms on the outer side are only shared by two octahedra. These outer oxygen atoms are hydrogen-bound to two other similarly coordinated oxygen atoms in the neighboring double layers above and below. The stacking of the layers is such that the hydroxyl groups of one layer are located over the depression of hydroxyl groups in the adjacent layer.

- **Pseudoboehmite** (**gelatinous boehmite**) contains higher amount of water than boehmite (γ-AlO(OH)$\cdot n$H$_2$O, where n ranges from 0.08 to 0.62) [339].

- **Doyleite** is triclinic Al(OH)$_3$ ($P\bar{1}$or P1,a=5.002 Å, b=5.175 Å, c=4.98 Å, α=97.5°, β=118.6, γ=104.74° and Z=2) polymorph of gibbsite, bayerite and nordstrandite. Doyleite was firstly described in 1985 [340].

- **Nordstrandite** (Fig.5(c)) is triclinic polymorph of Al(OH)$_3$ (P1, a=6.148 Å, b=6.936 Å, c=5.074 Å, α=79.76°, β=99.06, γ=83.3°) synthesized and identified by van Nordstrand at al. in 1956 [341][1]. This polymorph occurs in nature and can be prepared by the crystallization of alumina gels at high pH and the presence of chelating agent.

- **Diaspore** is orthorhombic α-AlO(OH) (*PBnm*, a=4.379 Å, b=9.421 Å, c=2.844 Å and Z=4) which is rare and occurs in the metamorphic and sedimentary bauxite ores.

- **Amorphous gel forms** precipitate from aluminium salts. According to applied conditions, various crystalline forms mentioned above can be prepared.

Some selected properties of Al(OH)$_3$ polymorphs including the point of zero charge are listed in Table 1. The experimental methods used to determine the PZC/IEP are described using the following abbreviations [343]:

- CIP (common intersection point) of potentiometric titration curves obtained at three or more ionic strengths or equivalent methods;

- Intersection (intersection point) of potentiometric titration curves obtained at two ionic strengths);

- pH (natural pH of the dispersion), e.g., mass titration and potentiometric titration at one electrolyte concentration;

- IEP (isoelectric point) obtained by means of electrophoresis, electroosmosis, or electroacoustic method.

---

1 Van Nordstrad proposed the name Bayerite II for this polymorph of Al(OH)3.

Phase	pH of PZC/ IEP	d001 [Å]	Density [g·cm^{-3}]	Al$_2$O$_3$ [%]	H$_2$O [%]
Gibbsite	8.1 – 9.8 (10) [342-344]	4.85	2.34		
Bayerite	5.4 – 9.7 [347] 8.1 [345] 9.2 [344]	4.79	2.53	65.4	36.4
Nordstrandite	?	4.72	2.42		
Doyleite	…	…	2.48		
Boehmite	7.3 – 7.5 [343] 8.9 [343] 9.4 [344]	6.12	3.03	85.0	15.0
Pseudoboehmite	9.2 [346,344]	…		77.7-84.0	16-22.3
Diaspore	7.9 [343] 6.9 – 8.8 [347]	…	3.38	85.0	15.0
Amorphous	9.4-9.5 [348]	…	…	…	…

Table 1. Properties of strontium aluminate polymorphs.

The thermal treatment of these compounds leads to the dehydration and subsequent formation of the most stable modification of α-Al$_2$O$_3$. The process is complicated due to the formation of different **transitional aluminas**. The industrial importance of transitional aluminas is the application of many phases as catalysts or carriers (support) for catalysts for petrochemical and fine chemical processes [349,350].
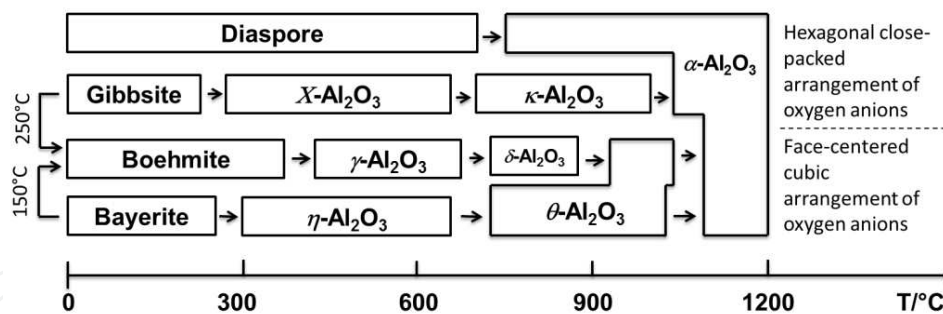
Figure 4. Temperature transformation of hydroxides or oxohydroxides to corundum via the formation of transitional alumina phases [325].

Significant effects of pH value on the composition, structure, morphology, and phase transformation of precipitated aluminium hydroxide can be observed. During the increase of pH value from 5 to 11, the aluminum hydroxides precipitating from the solution vary from amorphous aluminum hydroxide through γ-AlOOH to α-Al(OH)$_3$; and the corresponding morphology of the aluminum hydroxide particles changes from the ultrafine floccules through 50 nm blowballs up to irregular agglomerates with the average diameter of 150 nm. The aluminum hydroxides precipitating at different pH values have different transformation sequences toward α-Al$_2$O$_3$ and different formation temperatures of α-Al$_2$O$_3$ [351]:

- **Amorphous aluminum hydroxide** precipitating at the pH of 5-6 is transformed to α-Al_2O_3 at 950 °C via the following transformation sequence:

*Amorphous hydroxide $\rightarrow$ amorphous alumina $\rightarrow$ α-Al_2O_3*

- **Boehmite** precipitating at pH=7 transforms to α-Al_2O_3 at 950 °C via the following path:

γ-$AlOOH \rightarrow \gamma$-$Al_2O_3 \rightarrow \alpha$-$Al_2O_3$
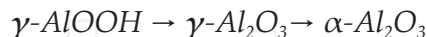
- **Bayerite** precipitating at the pH values between 8 and 11, is transformed to α-Al_2O_3 at 1000 °C via the transformation sequence:

α-$Al(OH)_3 \rightarrow \gamma$-$Al_2O_3 \rightarrow \varepsilon$-$Al_2O_3 \rightarrow \eta$-$Al_2O_3 \rightarrow \alpha$-$Al_2O_3$

The temperature relationships between transitional alumina phases are complicated. The course of the process depends on the type of initial hydroxide or oxohydroxide due to their structural similarities, experimental conditions and content of admixtures (Fig.4). Some uncertainty still remains about the numbers and transition sequence between these phases. The course of the phase transitions seems to be given by the requirement to attain the closest structural similarity between original and newly formed phase. The structural similarity between the structures of original and newly formed phase is termed as **topotaxy**. The final product of the process is α-Al_2O_3 in all cases.
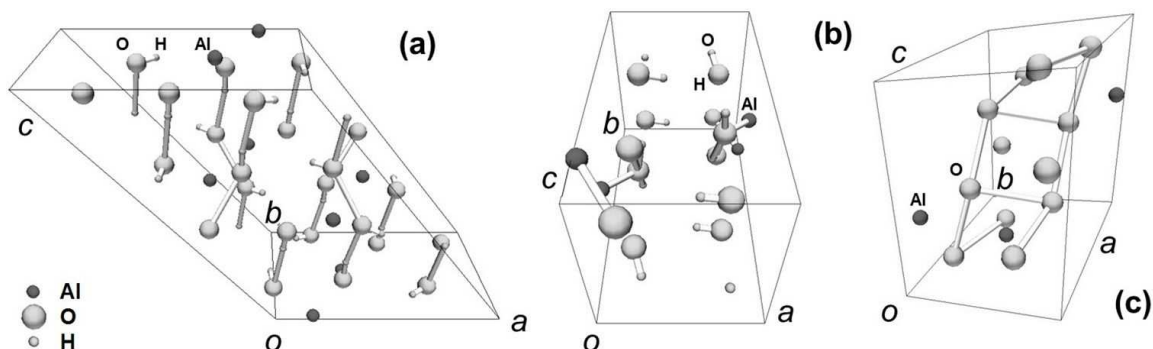
Figure 5. The structure of gibbsite (a), bayerite (b) and nordstrandite (c).

Two general groups of transitional alumina phases can be recognized [325]:

1.   **Transitional alumina with face-cantered cubic arrangement of oxygen anions** including cubic γ-Al_2O_3 (*gamma*) and η-Al_2O_3 (*eta*), monoclinic θ-Al_2O_3 (*theta*) and tetragonal (or orthorhombic) δ-Al_2O_3 (*delta*) polymorphs.

2.   **Transitional alumina with hexagonal close packed arrangement** where trigonal polymorph of α-Al_2O_3 (*alpha, corundum*), orthorhombic κ-Al_2O_3 (*kappa*) and hexagonal χ-Al_2O_3 (*chi*) are included.

Another classification of transitional alumina phases defines:

1.   **Low-temperature transition alumina phases** (γ-and η-Al_2O_3);

2.   High-temperature transition alumina phases (δ-and η-Al_2O_3).

The beta modifications of alumina including β-and β''-alumina (three blocks structure) are not polymorphs of Al_2O_3, but they are binary or more complex solid solutions of alumina with different metal ions. The beta alumina group of oxides has closely-packed slabs (spinel block) and loosely-packed layers (conduction planes) with mobile ions. The spinel block consists of four layers of oxygen ions with aluminium ions in both octahedral and tetrahedral interstices.
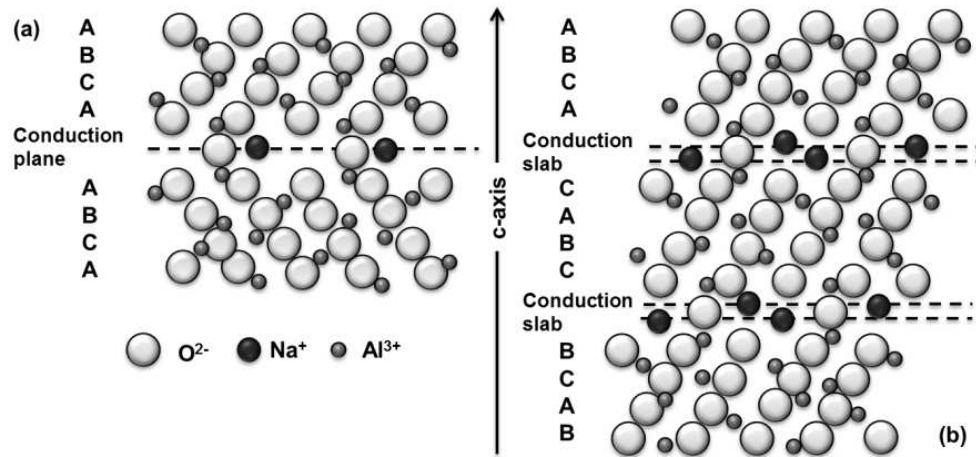
Figure 6. Stacking sequence of β' and β'' alumina in the unit cell shown in the (11 $\bar{2}$ 0) projection [**352**].

Two neighboring spinel blocks are bound via the conduction plane. There are two different crystal structures (Fig.6):

a.   **Hexagonalβ-alumina** ($P6_3$/mmc; a=0.559 nm, c=2.261nm) where the conduction plane is sandwiched in between two spinel blocks (two-block structure). The ideal formula of β-alumina is Na_2O $11Al_2O_3$.

b.   **Rhombohedralβ''-alumina** ($R3m$; a=0.560 nm, c=3.395 nm) where two conduction slabs are separated by three spinel blocks. Since they accommodate higher amount of sodium ions, the structure of β''-Al_2O_3 shows higher conductivity than β-Al_2O_3. The phase is stable up to the temperature of 1600 °C. The ideal formula of β''-alumina is Na_2O $(Al_2O_3)_{6+x}$.

These materials can be used as solid electrolytes (BASE), sodium heat engine or alkali metal thermoelectric converters for direct thermoelectric energy conversion, gas sensors, galvanic cells for the measurement of thermodynamic data [353-358].

From this viewpoint the following phases can be recognized:

• AM – β and/ orβ''-alumina where AM denotes Alkali Metals (Li, Na, K, Rb…). Sodium β-or β''-alumina (Na_2O_{1+x} $11Al_2O_3$ where x=0.25 – 0.55) exhibits high sodium conductivity at relatively low temperatures (300 – 350 °C). The most convectional technique for the production is solid-state synthesis based on the thermal treatment of Na_2CO_3 and α-Al_2O_3

mixture. Ion exchange in molten salt is further used for the preparation of other ion-alumina phases and their mixtures [359-361].

- AEM – β and/ orβ''-alumina where AE denotes Alkaline Earth Elements=Ca, Sr, Ba. The structure consists of two spinel block and an intermediate layer. Large cations such as Ba^{2+}occupy the nine-fold coordination sites in intermediate layer of b-alumina structure. Small cations, such as Sr^{2+}or $Ca^{2+}$are located in the twelve-fold coordination sites of MP structure in aluminum oxide [362].

- REE – β and/ orβ''-alumina where REE denotes Rare Earth Elements such as Gd^{3+}, Eu^{3+}, Nd^{3+} … [363]

- M – β and/ orβ''-alumina where Ag^+, Pb^{2+}mobile ions were used.

1.1. Influence of the source of alumina

It can be concluded that there are several ways to produce strontium aluminate clinker from raw material bases:

1. The mixture of strontium carbonate with alumina;

2. The mixture of strontium carbonate with transitional aluminas;

3. The mixture of strontium carbonate with aluminium hydroxides, oxohydroxides or gels;

4. The mixture of strontium carbonate with bauxite;

5. The advanced techniques.

Using alumina is promising way for the preparation of high purity product, where the course of solid state reaction (Eq.43), the phase composition and the properties of product can be easily controlled. Moreover, transition aluminas, hydroxides, oxohydroxides or gels have an advantage in higher reactivity.

Using bauxite may increase the content of Fe in the strontium aluminate cement which decreases the thermal stability of materials especially after the reduction conditions. In principle the same production process as for alumina cement can be used.

The activated aluminas, i.e. acidic, neutral and basic aluminas (no definite chemical compositions; made by adding various amounts of water to activated aluminas) are used extensively as adsorbents because of their affinity for water and other polar molecules; and as catalysts because of their large surface area and appropriate pore structure. As adsorbents, they are used for drying gases and liquids; and in adsorption chromatography. The catalytic properties may be attributed to the presence of surface active sites (primarily OH^-, O^{2-}, and Al^{3+}ions). Such catalytic applications include the sulphur recovery from H_2S (Clauss catalysis); the dehydration of alcohols, the isomerization of olefins; and as the catalyst support in petroleum refining [91].

Fig.7 shows the temperature dependence of the synthesis of molar unit of strontium aluminate phase using different sources of alumina. These results clearly indicate that γ-Al_2O_3 is the most reactive oxide form for the synthesis of strontium aluminate while thermodynamically most stable α-Al_2O_3 reacts less willingly. Aluminum hydroxides and oxide-hydroxides are even more reactive, but they are the subject of dehydroxylation and phase transformation before sufficient temperature is reached. Therefore we need to identify aluminium hydroxide or oxide-hydroxide which form γ-Al_2O_3 within the temperature interval where the formation of strontium aluminate proceeds.
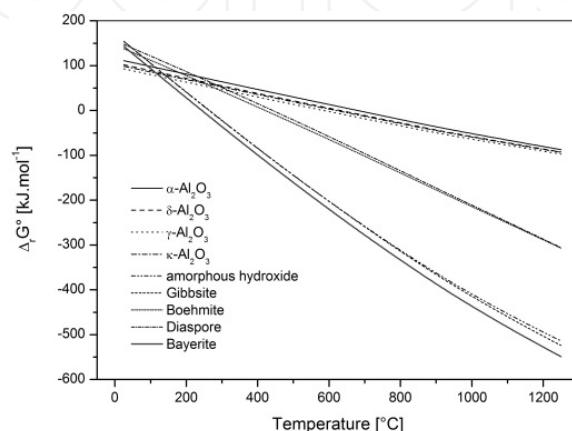

Figure 7. Temperature dependence of $\Delta_rG°$ for the formation of structure unit of $SrAl_2O_4$ from different sources of alumina.

Diaspore (α-AlO(OH)) is directly transformed to the lesser reactive form of α-Al_2O_3 (Fig.4) within the temperature range from 350 to 500 °C (please compare Fig.8(a) and (c)). From this viewpoint, it is not appropriate to use it for the synthesis. In the temperature interval where the formation of strontium aluminate takes place, the thermal transformations of gibbsite, bayerite and boehmite lead to κ-Al_2O_3, Θ-Al_2O_3 and δ-Al_2O_3, respectively.

These transitional alumina phases are all more reactive than corundum, but the question is which of the transitional alumina phases is the most reactive or which transition sequence is optimal and will prevail the for synthesis of strontium aluminate clinker. In the assumption that the phases which require the minimum structural changes (or have the highest structural similarity) are formed predominantly, the bayerite leading to the monoclinic Θ-Al_2O_3 should be considered as the most reactive phase. On the other hand, there is another factor such as alumina source availability. From this point of view, the gibbsite as the main product of Bayer process is promising raw material.

The course of synthesis of strontium aluminate clinker can be significantly changed by the source of Al_2O_3. Regardless of raw material prices, the usage of thermodynamically most stable modification of α-Al_2O_3 (corundum[2]) as the source of aluminium oxide requires the highest temperatures and the longest time for the synthesis.

---

2 Corundum for ceramics purposes is often produced from bauxite via Bayer process (Chapter 2.1.2).
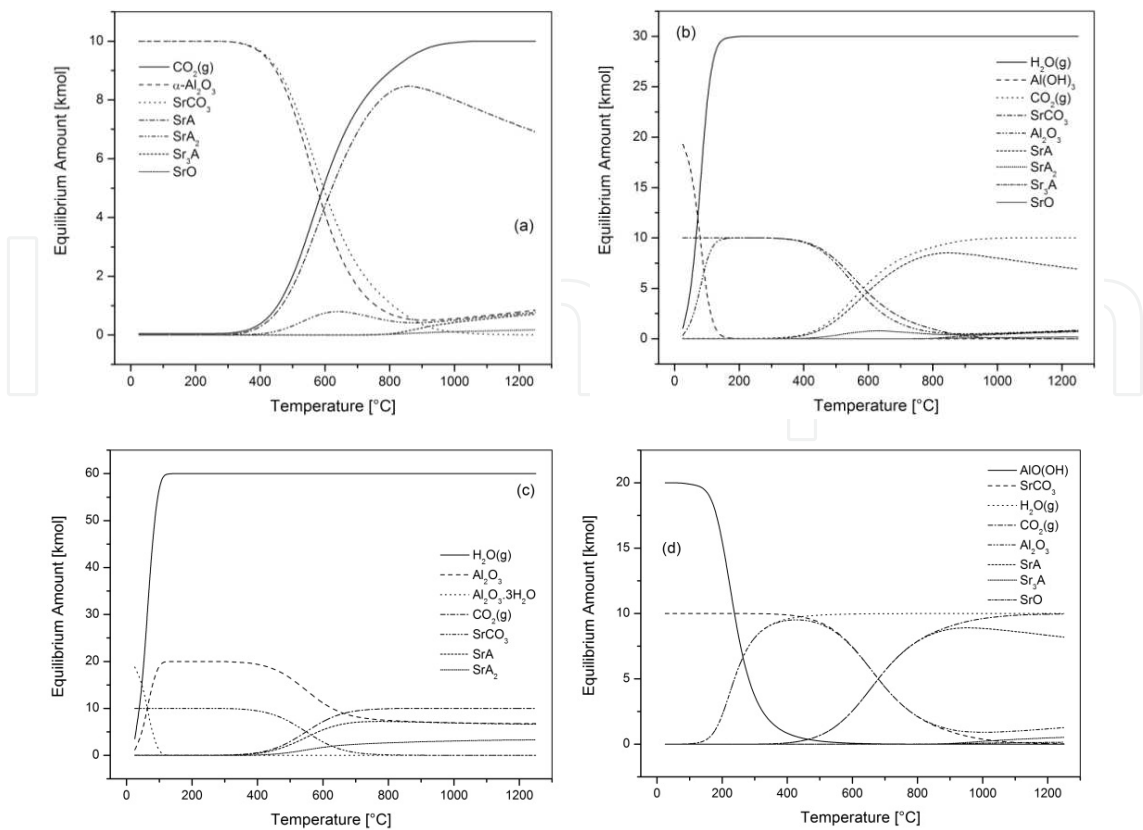
Figure 8. Formation of strontium aluminate clinker from the mixture of $SrCO_3$ with corundum (a), gibbsite, bayerite (c) and diaspore (d)

1.2. Thermal decomposition of Al(OH)₃

Thermal decomposition of gibbsite can be described by the reaction [364,365]:

$$2 \, Al(OH)_3(s) \rightarrow Al_2O_3(s) + 3 \, H_2O(g) \tag{1}$$

The published data related to the kinetic triplet, which includes the activation energy, the frequency factor and the kinetic factor of the process, are listed in Table.2.

Kinetic triplet data			Note		Reference
E_a [kJ·mol⁻¹]	A [s⁻¹]	n			
108.5	2.93·10⁹	~1	Gibbsite	Kissinger Equation	[365]
198	---	---	Boehmite	Staring Equation	[368]
175	1.20•10⁹	$m = 0,205$ $n = 0,738$	Diaspore	Šesták-Berggren	[366]

Table 2. Thermal decomposition of aluminas.

It is generally accepted that hydrothermal conditions favor the formation of boehmite from gibbsite. The pathway of the dehydration is affected by the particle size, partial pressure of water vapor and heating rate. On the contrary to the dehydration sequence in Fig.4, there are at least three ways for the dehydration of gibbsite [367]:

a.   Small crystals (< 10 μm) in dry air at atmospheric pressure;

b.   Large crystal (> 100 μm) in wet air under the pressure higher than atmospheric;

c.   Flash calcination of gibbsite.

This transformation sequences are shown in Fig.9.
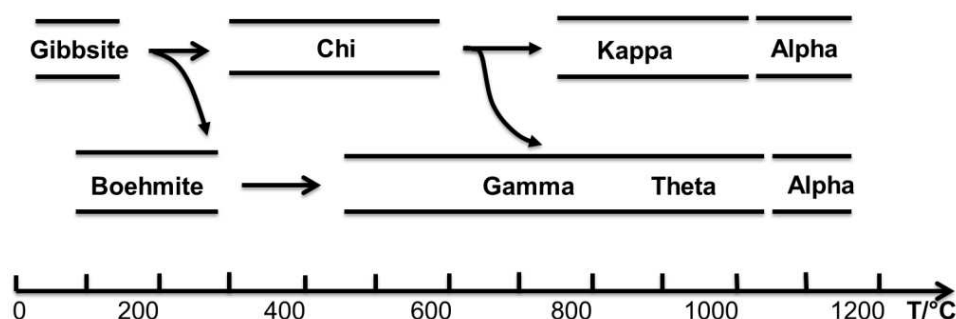
Figure 9. Influence of conditions on the reaction pathway for the dehydration of gibbsite [367].

When mechanically activated by vigorous grinding, many crystalline materials, including gibbsite, are known to lose their long-range order and become X-ray amorphous. Amorphous phase retains its water content and becomes "gel-like". The thermal dehydration of this amorphous phase broadens the characteristic gibbsite dehydroxylation endotherm and lowers its temperature to about 150 – 200°C. The dehydrated product is also X-ray amorphous and is thermally converted to α-alumina (Fig.4) either via η-alumina or via the γ-δ-η sequence [364].

The dehydration of boehmite is a topotactic process, which can be described by the following decomposition reaction [73,368]:

$$2\,AlOOH(s) \rightarrow Al_2O_3(s) + H_2O(g) \tag{2}$$

The mechanism of boehmite transformation to γ-Al$_2$O$_3$ involves the elimination of water formed by protons and hydroxyl groups and the migration of Al cations. The latter is the rate-limiting step.

2. Thermal decomposition of strontium carbonate

The thermal decomposition of strontium carbonate should be described by simple first order chemical equation:

$$\alpha\text{-}SrCO_3(s) \xrightarrow{\ 930°C\ } \beta\text{-}SrCO_3(s) \xrightarrow{\ T\ } SrO(s)+CO_2(g) \tag{3}$$
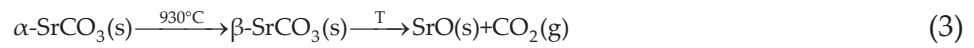
From the thermodynamic point of view, there is only simple chemical reaction in the system:

$$\sum_{i=1}^{N} v_i C_i = 0 \tag{4}$$

where v_i is the stoichiometric coefficient for species C_i. According to the convection:

• The value of $v_i < 0$ for reactants;

• The value of $v_i > 0$ for products;

• The value of $v_i=0$ for specimens which do not participate in the reaction.

The change in the number of moles for the reaction 4 is then equal to Σv_i.

Since pure condensed phases ($SrCO_3$ and SrO) which participate in reaction 3 do not form solid solution, their activities are equal to one ($a_{SrCO3}=1$ and $a_{SrO}=1$) if pure solid phase at given temperature and pressure is considered as standard state. In the other words, the activities of condensed phases do not influence the value of equilibrium constant and Σv_i includes gas species (CO_2) only.

The Gibbs energy (G) of open homogeneous system is described by the general equation:

$$G = f(T,p,n_1,n_2,...n_i) \tag{5}$$

where T is the temperature, p is the pressure and n_1, n_2,...n_i denote the number of moles of chemical species of the reaction system. The expression for total differential of Eq.5 is given as the following relation:

$$dG = \left(\frac{\partial G}{\partial T}\right)_{p,n_i} dT + \left(\frac{\partial G}{\partial p}\right)_{T,n_i} dp + \sum \left(\frac{\partial G}{\partial n_i}\right)_{p,T,n_{j\neq i}} dn_i \tag{6}$$

Based on the relations:

$$\left(\frac{\partial G}{\partial T}\right)_{p,n_i} = -S ; \quad \left(\frac{\partial G}{\partial p}\right)_{T,n_i} = V ; \quad \left(\frac{\partial G}{\partial n_i}\right)p,T,n_{j\neq i} = \mu_i \tag{7}$$

Eq.6 can be written as:

$$dG = -S\ dT + V\ dp + \sum \mu_i dn_i \tag{8}$$

$$dG = -S\, dT + V\, dp + \sum \mu_i \nu_i\, d\xi \tag{9}$$

where μ_i is the chemical potential, $dn_i = \nu_i\, d\xi$ and ξ is the extent of the reaction. For complete chemical reaction where ν_i mols of species i react, the value of $d\xi = 1$.

The equilibrium state is required to fulfill the following conditions:

$$dG_{T,p} = 0 \tag{10}$$

$$\sum_i \nu_i \mu_i = 0 \tag{11}$$

From the consideration mentioned above the Gibbs energy of chemical reaction reaches the minimum for the equilibrium state and should be written as:

$$\Delta_r G = \left(\frac{\partial G}{\partial \xi}\right)_{T,p} = \sum \frac{\partial G}{\partial n_i}\frac{\partial n_i}{\partial \xi} = \sum \nu_i \mu_i = 0 \tag{12}$$

where $dn_i/d\xi = \nu_i$. The chemical potential is defined as follows:

$$\mu_i = \mu_i^{\circ} + RT \ln a_i \tag{13}$$

where μ_i° is the standard chemical potential and a_i is the activity. For the standard state, the value of $a_i = 1$ and $\mu_i = \mu_i^{\circ}$. From the combination of Eqs.12 and 13 follows:

$$\Delta_r G = \sum \nu_i \mu_i^{\circ} + RT \sum \nu_i \ln a_i = 0 \tag{14}$$

$$\Delta_r G = \Delta_r G^{\circ} + RT \sum \nu_i \ln a_i = 0 \tag{15}$$

$$\Delta_r G^{\circ} = -RT \sum \nu_i \ln a_i \tag{16}$$

$$\Delta_r G^{\circ} = -RT \ln \prod a_i^{\nu_i} = -RT \ln K \tag{17}$$

$$K = \exp\left(\frac{-\Delta_r G}{RT}\right) \tag{18}$$
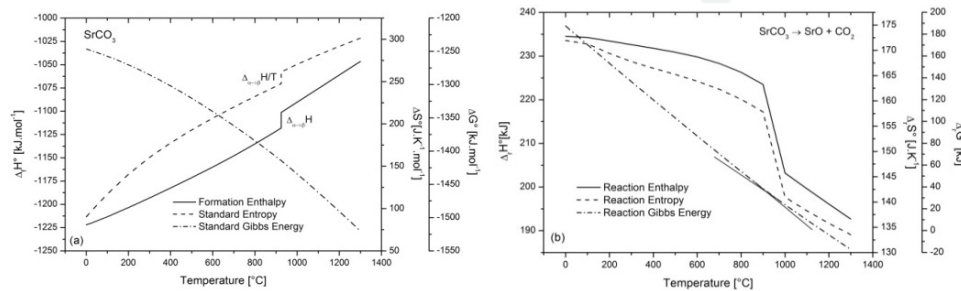
where K is the equilibrium constant of reaction 4.

From the definition of Gibbs energy:

$$G = H - TS \tag{19}$$

where H and S are enthalpy and entropy, the law for reaction Gibbs energy can then be written as:

$$\Delta_r G^\circ = \Delta_r H^\circ - T \Delta_r S^\circ \tag{20}$$

Figure 10. Temperature dependence of the thermodynamic potentials for species (a) and reaction (b).

The temperature dependence of $\Delta_r G^\circ$ (Fig.10) can be calculated using the following equations:

$$\Delta_r H^\circ(T_2) = \Delta_r H^\circ(T_1) + \int_{T_1}^{T_{\alpha \to \beta}} \Delta c_p^\alpha \, dT + \Delta_{\alpha \to \beta} H^\circ + \int_{T_{\alpha \to \beta}}^{T_2} \Delta c_p^\beta \, dT \tag{21}$$

$$\Delta_r S^\circ(T_2) = \Delta_r S^\circ(T_1) + \int_{T_1}^{T_{\alpha \to \beta}} \frac{\Delta c_p^\alpha}{T} \, dT + \frac{\Delta_{\alpha \to \beta} H^\circ}{T_{\alpha \to \beta}} + \int_{T_{\alpha \to \beta}}^{T_2} \frac{\Delta c_p^\beta}{T} \, dT \tag{22}$$

where $\Delta_r H^\circ$ and $\Delta_r S^\circ$ are the standard reaction enthalpy and entropy, respectively, $\Delta_{\alpha \to \beta} H^\circ$ and $\Delta_{\alpha \to \beta} H^\circ / T = \Delta_{\alpha \to \beta} S^\circ$ are the enthalpy and entropy related to the $\alpha \to \beta$ phase transformation and Δc_p is the isobaric heat capacity:

$$\Delta c_p = \left(\frac{\partial \Delta_r H^\circ}{\partial T} \right)_p = \sum_i \nu_i c_{p,i} \tag{23}$$

The temperature dependence of heat capacity is given by law:

$$c_{p,i} = A + BT + \frac{C}{T^2} + DT^2 \tag{24}$$

Where A, B, C and D are the constants for given species.

Another option for the calculation of dependence of $\Delta_r G°$ is to use the equation which was derived from Eq.20:

$$\left(\frac{\partial \frac{\Delta_r G°}{T}}{\partial T}\right)_p = -\frac{\Delta_r H°}{T^2} \tag{25}$$

The activity of the ideal mixture of gasses is given by the following relation:

$$a_i = \frac{P_i}{P°} = \frac{P \, x_i}{P°} = P^* x_i \tag{26}$$

where P^*, $P°$, P and P_i are the relative pressure, the standard pressure, the pressure and the partial pressure which is given by the Dalton law ($P_i = P \bullet x_i$) and $x_i = n_i / \Sigma n_j$. Therefore, the value of K should be expressed as follows:

$$K = \prod_i x_i^{v_i} P^{*\sum_i v_i} = \prod_i n_i^{v_i} \left(\frac{P^*}{\sum_j n_j}\right)^{\sum_i v_i} \tag{27}$$

The thermodynamic equilibrium constant of the process 3 is then:

$$K = n_{CO_2} \frac{P^*}{n_{CO_2}} = P^*_{CO_2} \tag{28}$$

Therefore the following can be derived:

$$\Delta_r G° = -RT \ln K = -RT \ln p^*_{CO_2} \tag{29}$$

In order to explain the influence of temperature and relative pressure of carbon dioxide on the thermal stability of $SrCO_3$ as well as other carbonates that are important for the chemistry of strontium aluminate cement (Fig.11) was constructed. For this purpose, the following type of reaction is supposed:

$$MeO + CO_2 \rightarrow MeCO_3 \text{ , where } Me = Ca, Mg, Sr, Ba, Fe \ldots \tag{30}$$

All reactions are balanced for 1 mol of CO_2 hence the standard Gibbs energy for the reaction is given by the formula:

$$\Delta_r G^\circ = RT \ln P^*_{CO_2} \qquad (31)$$

The value of Gibbs energy which is necessary for one mol of CO_2 to expand from standard to the equilibrium pressure related to given temperature is:

$$\Delta G = -RT \ln \frac{P}{P^\circ} = -RT \ln P^* = -(R \ln P^*) T \qquad (32)$$

The lines representing the constant relative pressure form the $P^*_{CO_2}$ scale of diagram in Fig.11.
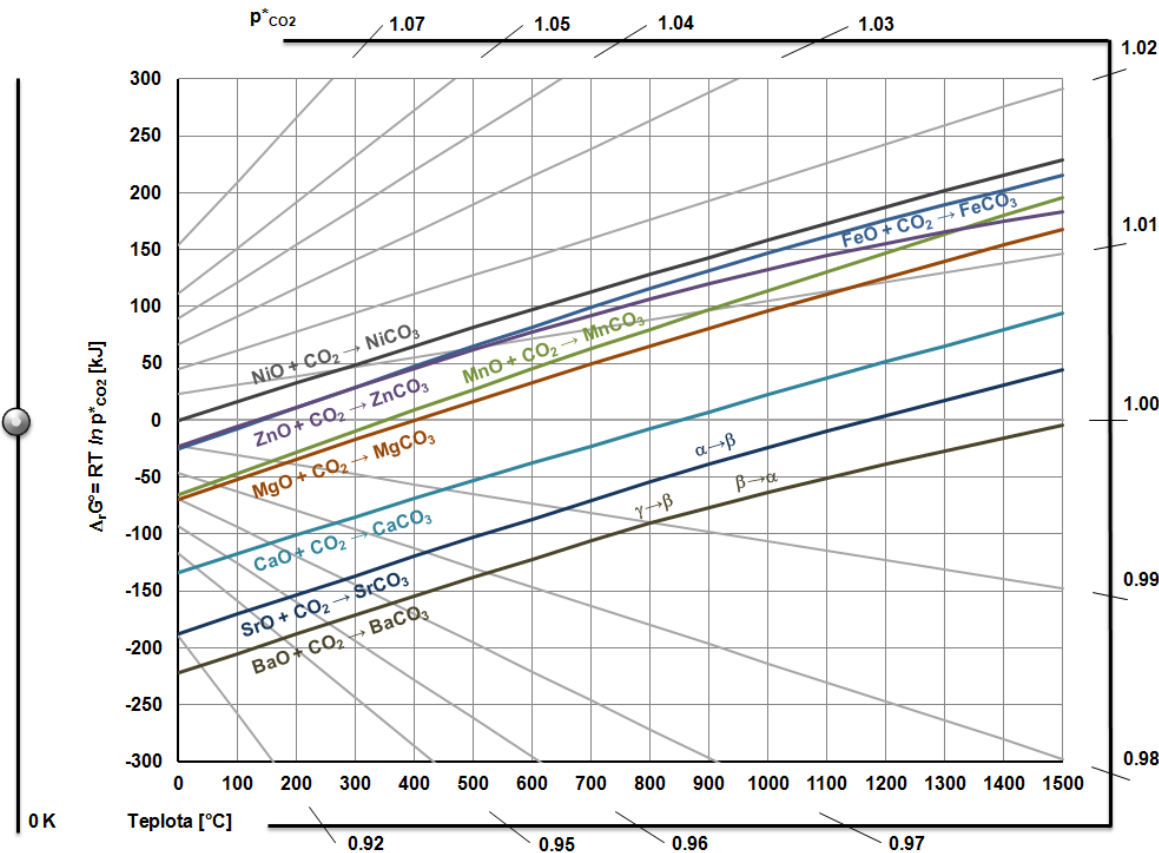

Figure 11. Thermal stability of carbonates.

The temperature of spontaneous thermal decomposition of carbonate can be found as the cross point of the temperature dependence of $\Delta_r G^\circ$ with the line for $P^*_{CO_2}=1$. For strontium carbonate we can read the temperature of 1175 °C. The change in line direction means the

phase transformation. Strontium carbonate shows the transformation of orthorhombic (α) to hexagonal (β) modification at 925 - 935 °C. From the diagram we can read the value which is necessary for the thermal decomposition of $SrCO_3$, below the temperature of phase transformation. The extrapolation of line between the point on the *0K* axis and the point on the temperature dependence of $\Delta_rG°$ for 925 °C to the axis of relative pressure of CO_2 provides the value of 0.9965. Therefore the partial pressure of CO_2 lower than 100.97 kPa is needed. On the contrary, the equilibrium temperature of thermal decomposition can be increased by increasing the value of $P^*_{CO_2}$. For example, for the temperature of 1400 °C the attainment of $P^*_{CO_2}$ of 1.002, i.e. the partial pressure of 101,53 kPa is required.

In some cases the cross point between the temperature dependences of $\Delta_rG°$ for two carbonates occurrs which means the chemical reaction. For example, at the temperature of 1330 °C there is an equilibrium of two reactions under $P^*_{CO_2}$ = 1.013 :

$$MnO + CO_2 \rightarrow MnCO_3 \quad \text{(a)} \tag{33}$$

$$ZnO + CO_2 \rightarrow ZnCO_3 \quad \text{(b)} \tag{34}$$
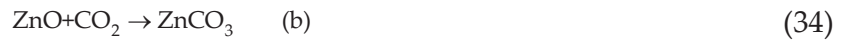
Therefore the following reaction can be supposed:

$$ZnO + MnCO_3 \rightarrow MnO + ZnCO_3 \quad \text{(c)} \tag{35}$$

$$\Delta_rG°(c) = \Delta_rG°(b) - \Delta_rG° \quad \text{(a)} \tag{36}$$

The value of $\Delta_rG°(c) > 0$ below the equilibrium temperature (reaction 35 shows opposite direction), while $\Delta_rG°(c) < 0$ if the temperature is higher than 1330 °C.

The reaction 3 shows that the phase transformation of orthorhombic α-$SrCO_3$ to the hexagonal structure of β-$SrCO_3$ proceeds prior to the thermal decomposition of strontium carbonate. This process shows sharp endothermic effect which is well visible at DTA (Fig.12). The equilibrium of both phases means that:

$$\mu^\alpha = \mu^\beta \Rightarrow d\mu^\alpha = d\mu^\beta \Rightarrow dg^\alpha = dg^\beta \Rightarrow dg = 0 \tag{37}$$

where:

$$dg^\alpha = -s^\alpha \, dT + v^\alpha \, dp \tag{38}$$

$$dg^{\beta} = -s^{\beta}\ dT + v^{\beta}\ dp \tag{39}$$

From that the Clapeyron law can be derived:

$$-s^{\alpha}\ dT + v^{\alpha}\ dp = -s^{\beta}\ dT + v^{\beta}\ dp \tag{40}$$

$$(s^{\beta} - s^{\alpha})\ dT = \frac{\Delta_{\alpha \to \beta} h}{T}\ dT = (v^{\beta} - v^{\alpha})\ dp \tag{41}$$

$$\frac{dp}{dT} = \frac{\Delta_{\alpha \to \beta} h}{T\ \Delta v} \tag{42}$$

2.1. Kinetics of thermal decomposition of SrCO$_3$

The behaviour of pure strontium carbonate during the thermal treatment is discussed in this chapter. The mechanism, the kinetics and the thermodynamic stability of activated complex of the process of thermal decomposition were assessed by non-isothermal TG-DTA and EGA assessment using the model-free Kissinger kinetic approach (Eq.112 in Chapter 1). 30 mg of strontium carbonate were heated to the temperature of 1200 °C using the heating rate from 5 to 25 °C min^{-1}. The kinetics of the process was evaluated from the shift of DTA peak with the heating rate[3]. It should be pointed that the peak temperature is higher than the temperature of $\alpha \to \beta$ transformation, therefore the kinetics results are related to the thermal decomposition of high temperature (hexagonal) polymorph of SrCO$_3$.
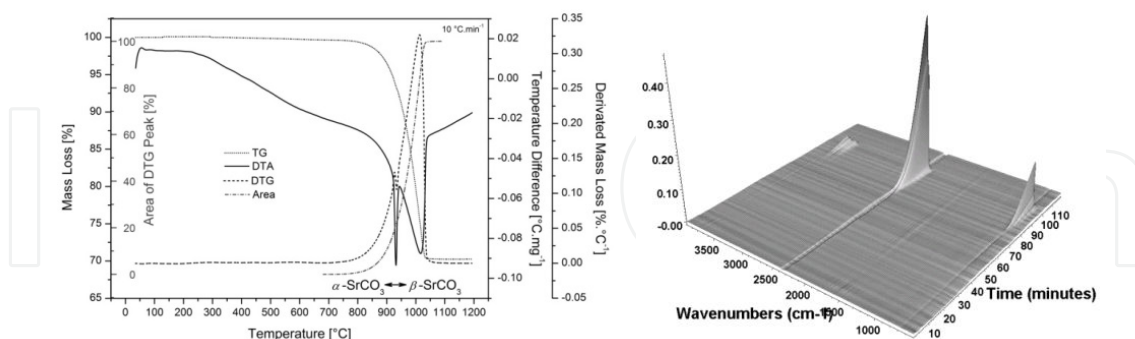

Figure 12. Typical plot of simultaneous TG-DTA and EGA analysis of strontium carbonate.

The slope of Kissinger plot (Fig.13(a)) enables to calculate the activation energy for the thermal decomposition of strontium carbonate (Eq.3) to be 223.7 kJ mol^{-1}. The kinetic factor was calculated according to the relation in Eq.113 in Chapter 1. The mechanism of the process was

---

3 Other options are to use the peak temperature of DTG or the EGA peak.

determined from the value of kinetic factor (n=2.73 ± 0.03) obtained via the extrapolation of the dependence of n on Θ to the nearly isothermal conditions ($\Theta \to 0$). The frequency factor can be then calculated from the intercept of Kissinger plot with y-axis to be 1.13 10^7 s^{-1}.
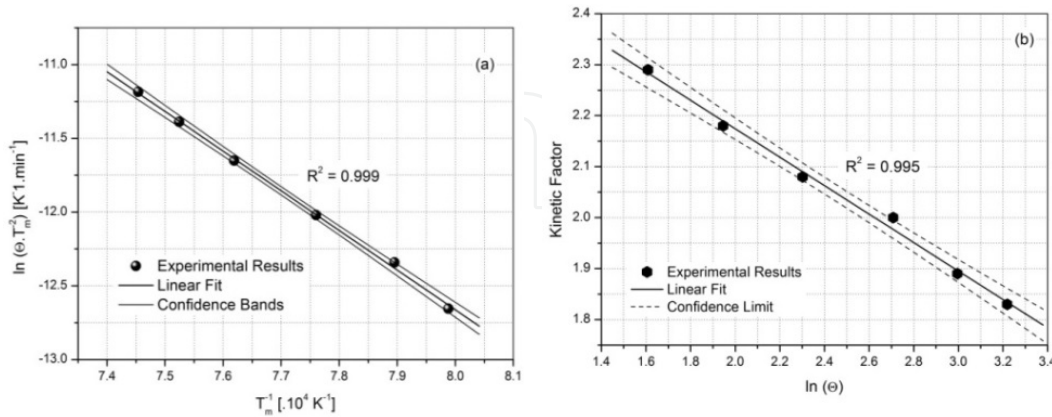
Figure 13. Kissinger plot (a) and extrapolation of kinetic factor to nearly isothermal conditions of the process (b).

The kinetics should be determined via the model fitting procedure using EGA data[4] as well. The total Gram-Schmidt reconstruction data show sharp peak related to the thermal decomposition of strontium carbonate. The peak was integrated and used to calculate the degree of conversion.
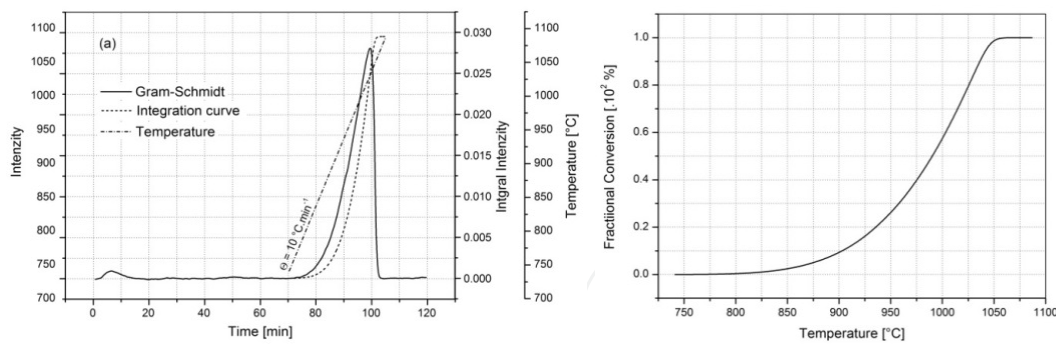

Figure 14. Using EGA to evaluate the kinetics of thermal decomposition of $SrCO_3$.

The rate determining step of the thermal decomposition of $SrCO_3$ is recognized from the slope of the dependence of $ln\,(g(\alpha)/T^2)$ on reciprocal temperature (Fig.15) as the rate of reaction on the reaction interface of contracted sphere (shrinking core, R_3: $1-(1-\alpha)^{1/3}$). The activation energy required for decarbonation of $SrCO_3$ has the value of 238.6 kJ.mol^{-1}. The frequency factor that was calculated from the intercept is 2.32 10^6 s^{-1}. Since usual error in the assessment of activation

---

4 Another and more often applied option is to use TG data in order to evaluate the kinetics of the process. On the other hand, there is one great advantage of EGA, as it is possible to monitor the required product (e.g. H_2O, CO_2, organics such as hydrocarbons, acetone, etc.) according to the selected wavelength.

energy usually reaches few percents of the determined value, the good agreement with the model free and model fitting method has been achieved.
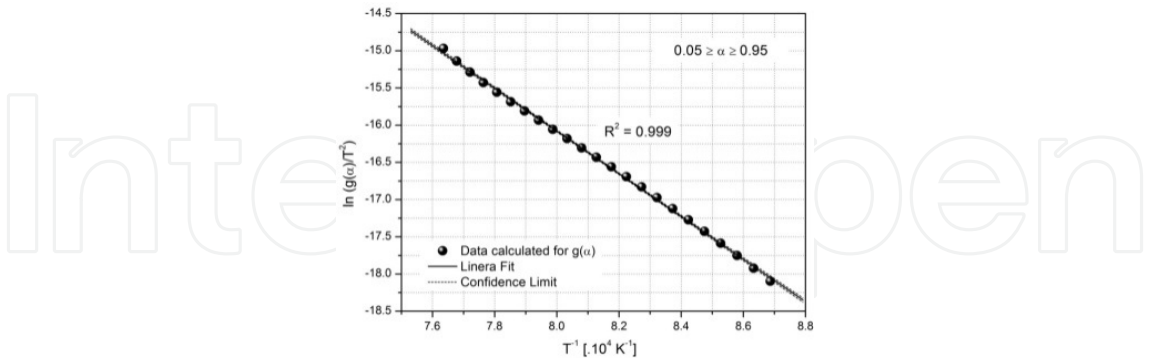
Figure 15. Determination of the activation energy for the most probable mechanism of the process.

These results are also in agreement with experimental as well as calculated[5] results published in literature, namely 233 and 238.7 kJ mol^{-1} [369], respectively.

### 2.2. Calculation of activation energy from thermodynamic data

The thermodynamic data required for the calculation of theoretical value of activation energy and the values of calculated equimolar (E_a^{Te}) and isobaric activation energy (E_a^{Ti}) for the process of thermal decomposition of strontium carbonate are listed in Table 3.

Parameter	Species	Temperature [K]				
		1000	**1100**	**1200**	**1300**	**1400**
$\Delta_f H°$ [kJ•mol^{-1}]	$SrCO_3(s)$	-1144.481	-1131.506	-1100.920	-1086.320	-1071.720
	$SrO(g)$	11.895	15.638	19.403	23.202	27.050
	$SrO(s)$	-556.539	-551.283	-546.023	-540.759	-535.482
	$CO_2(g)$	-360.097	-354.601	-349.006	-343.328	-337.580
$\Delta_r H°$	Eq.121 in Chapter 1	796.297	792.542	771.317	766.194	761.190
$\Delta_c H°$	$SrO(g{\to}s)$	-568.435	-566.920	-565.426	-563.961	-562.532
$\Delta_{rc} H°$	Eq.121 in Chapter 1	512.062	509.083	488.604	484.214	479.924
E_a^{Te}	Eq.121 in Chapter 1	256	255	244	242	240
E_a^{Ti}		512	509	489	484	480

Table 3. Thermodynamic data for the calculation of theoretical value of activation energy.

---

5 The method for the calculation of theoretical value of activation energy is described in Chapter 1.6.5. and the example in the next Chapter.

The schematic energy curve in Fig.16 illustrates the method used for the estimation of activation energy for the thermal decomposition of strontium carbonate according to congruent dissociative vaporization mechanism.
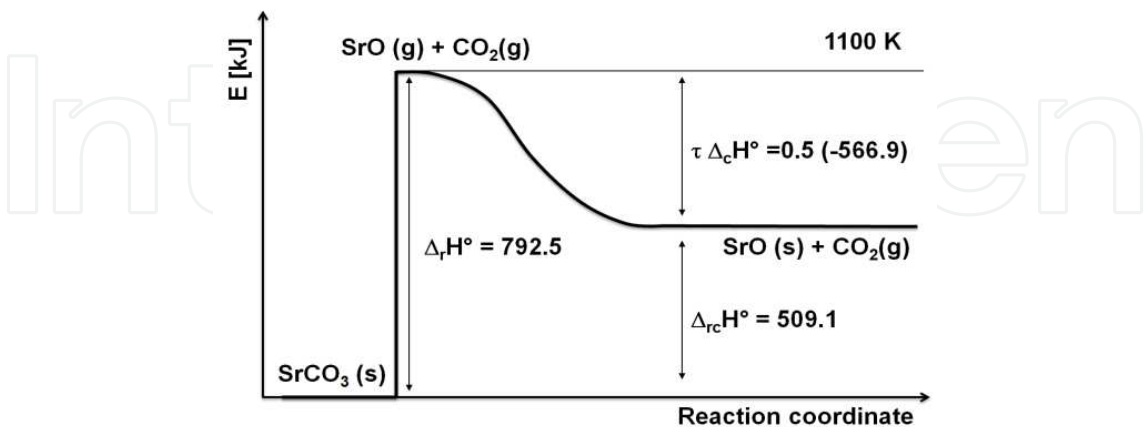
Figure 16. Schematic representation of energy curve for the thermal decomposition of $SrCO_3$.

The temperature dependence of equimolar activation energy on the heating rate is shown in Fig.17. The transitions between individual carbonate polymorphs lead to the step change in the value of activation energy.
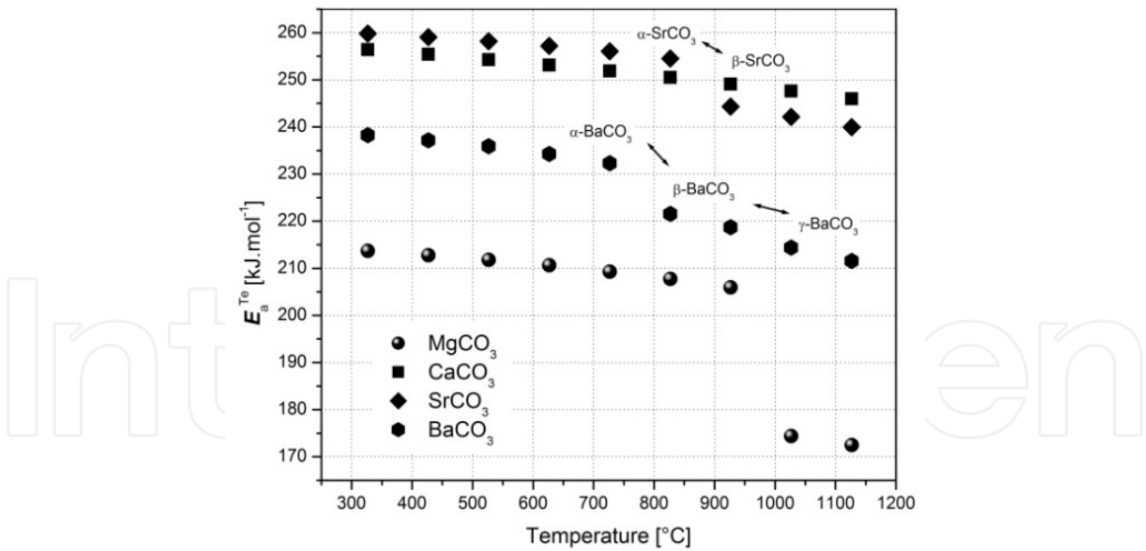
Figure 17. Dependence of E_a^{Te} on temperature.

2.3. Thermodynamics of thermal decomposition

The thermodynamic parameters of activated complex were calculated from Eqs.117 – 120 in Chapter 1 and are listed in Table 4.

T	$\Delta H^{\#}$	$\Delta S^{\#}$	$\Delta G^{\#}$	$K^{\#}$	v	k
[K]	[J·mol⁻¹]	[J·K⁻¹·mol⁻¹]	[J·mol⁻¹]			[s⁻¹]
295.15	221.24	-123.99	251.86	$8.41 \cdot 10^{-45}$	$6.22 \cdot 10^{12}$	$5.23 \cdot 10^{-32}$
1000	215.42	-128.48	343.34	$1.16 \cdot 10^{-18}$	$2.09 \cdot 10^{13}$	$2.42 \cdot 10^{-5}$
1100	214.59	-129.12	356.38	$1.19 \cdot 10^{-17}$	$2.29 \cdot 10^{13}$	$2.73 \cdot 10^{-4}$
1200	213.76	-129.76	369.42	$8.30 \cdot 10^{-17}$	$2.50 \cdot 10^{13}$	$2.08 \cdot 10^{-3}$
1300	212.93	-130.40	382.46	$4.29 \cdot 10^{-16}$	$2.71 \cdot 10^{13}$	$1.16 \cdot 10^{-2}$
1400	212.10	-131.34	395.50	$1.75 \cdot 10^{-15}$	$2.92 \cdot 10^{13}$	$5.11 \cdot 10^{-2}$

Table 4. Thermodynamic data of activated complex.

The plot of *ln k* vs $1/T$ of course gives the Arrhenius plot with the same activation energy (Fig. 18) as was calculated by Kissinger method. Therefore non-isothermal data can be used to calculate the isothermal rate constant (*k*) of the investigated process.
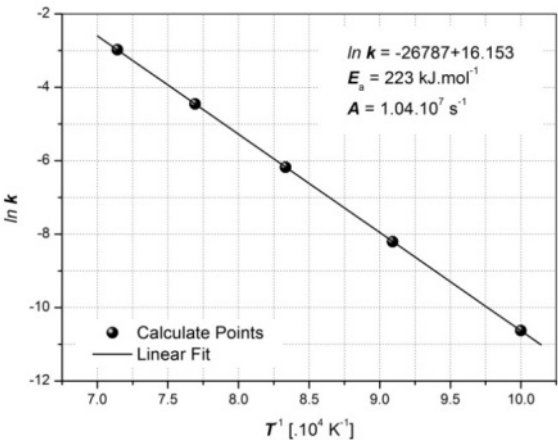

Figure 18. Arrhenius plot calculated from the data of activated complex.

3. Formation of strontium aluminate

During the early stages of sintering, mono-strontium aluminate is formed by the solid-state reaction between strontia and alumina in the powder compact:

$$SrCO_3 + Al_2O_3 \rightarrow SrAl_2O_4 + CO_2(g) \tag{43}$$

Hexaaluminate must be formed by further reaction of strontium aluminate (SrA) and alumina. That can proceed by two distinct mechanisms as is shown in Fig.19.
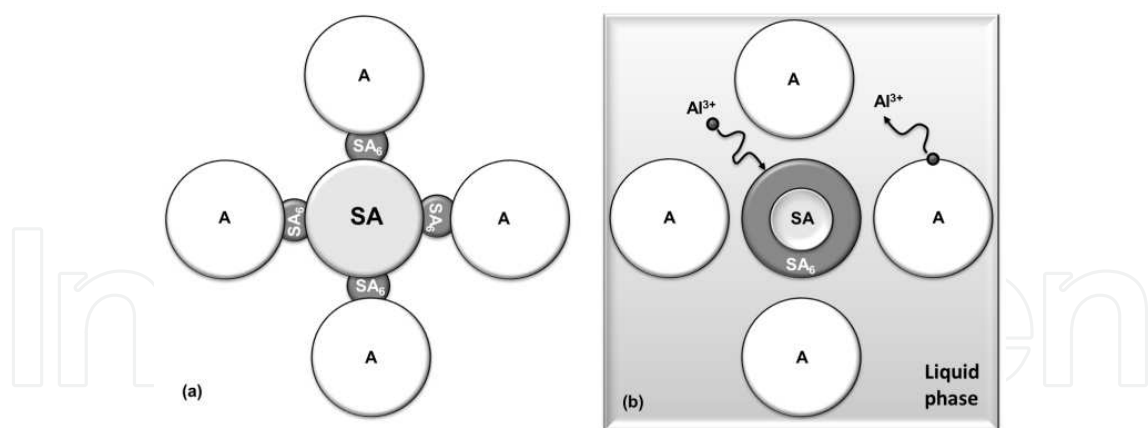
Figure 19. Mechanism of formation of strontium heaxaaluminate [371].

One possibility is that SrA_6 nucleates at the interfaces between alumina and SrA particles and the reaction proceeds by solid-state diffusion through the reactant phase. However, if the surfaces of SrA_6 and alumina grains are already wet by a liquid phase, the transformation to SrA_6 would, by necessity, proceed via the solution-precipitation reaction. The reaction by solid-state diffusion results in the formation of equiaxed SrA_6 grains, while the solution-precipitation favors the development of plate like grains. It is proposed that localized melting take place as a result of low temperature eutectic reaction in the $SrO-Al_2O_3$ system and it is the eutectic liquid which plays a dominant role in affecting the SrA_6 reaction mechanism (similar model is proposed by An et al. [370] for the alumina–calcia system) [371].

The difference in the final microstructure lies in the extent to which the solid-state reaction occurs between SrA and SrA_6 prior to wetting by liquid phase. This depends on a variety of factors including the particle size, the packing density and the uniform dispersion (mixing) of alumina–strontia powders. Just a slight difference in the above factors could have an appreciable effect on the subsequent wetting behaviour and the microstructure development. SrA_6 may be formed by the process [371]:

- Reaction between Sr and A:

$$Sr+6\,A \rightarrow SrA_6 \tag{44}$$

- Reaction between SrA and A:

$$SrA+5\,A \rightarrow SrA_6 \tag{45}$$

- Reaction between SrA_2 and A:

$$SrA_2 + 4\,A \rightarrow SrA_6 \tag{46}$$

- Reaction between SrA, SrA$_2$ and A:

$$SrA + SrA_2 + 9\,A \rightarrow 2\,SrA_6 \tag{47}$$

$$2\,SrA + SrA_2 + 14\,A \rightarrow 3\,SrA_6 \tag{48}$$

The phases SA and SA$_2$ are both the reaction intermediates and are minimized with the formation of SA$_6$. Similar reaction intermediates were proposed for the formation of calcium aluminates [371].

3.1. Thermal treatment of raw meal

The processes occurring during the formation of strontium aluminate clinker can be observed by HT-XRD analysis of raw meal upon heating. Fig.20 shows the changes in the phase composition of equimolar mixture of strontium aluminate and alumina. The diffraction lines of SrCO$_3$ start disappearing at the temperature of 800 °C. SrO formed via the thermal decomposition of SrCO$_3$ reacts with alumina and the diffraction line of tristrontium aluminate appears at 825 °C. For this reason the diffraction lines of alumina disappear at the same temperature
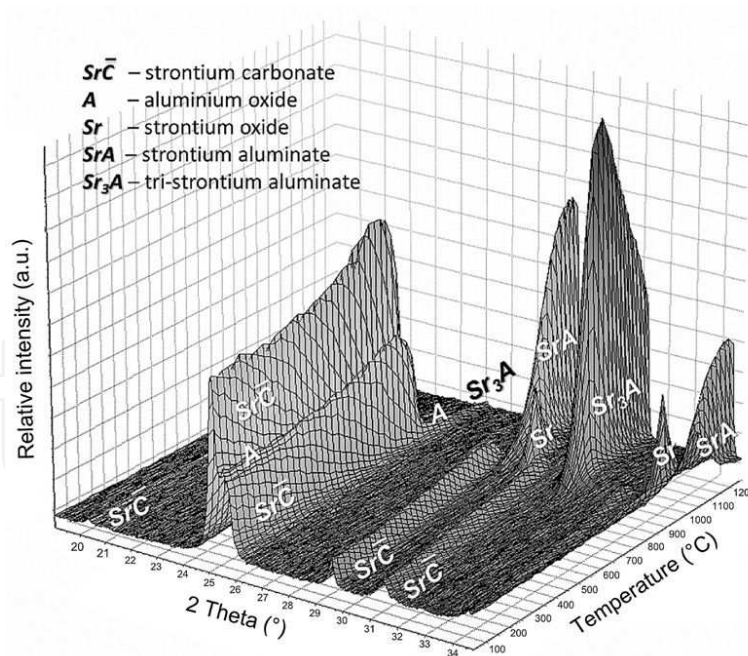
Figure 20. High-temperature X-ray diffraction analysis of raw materials upon heating with the heatinf rate of 10 °C min^{-1} [379].

The features of the main clinker phase, i.e. strontium aluminate, are recognized at the temperature of 875 °C. The process of thermal decomposition of strontium carbonate is not finished

yet and its diffraction lines can be detected up to the temperature of 1000 °C. The features of free SrO gradually disappear at the temperature of 1250 °C.

The comparison of X-ray diffraction pattern of raw materials (a) and fired strontium aluminate clinker (b) is shown in Fig.21. There are two main product of thermal treatment of raw equimolar mixture of $SrCO_3$ with Al_2O_3 to the temperature of 1600 °C, namely strontium aluminate and tri-strontium aluminate. Using quantitative X-ray diffraction Rietveld analysis, the content of strontium aluminate and tri-strontium aluminate phase in prepared strontium aluminate clinker is assessed to be 96 % and 4 %, respectively.
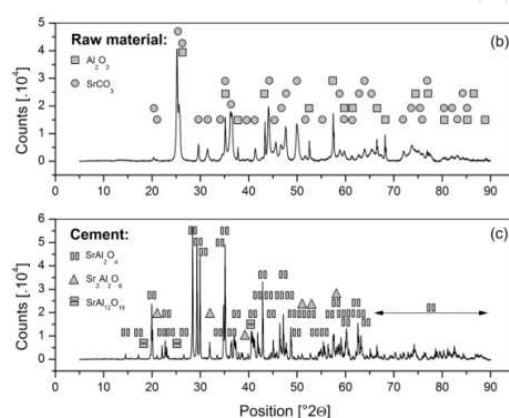
Figure 21. Initial (a) and final composition (b) of strontium aluminate clinker [379].

The comparison of infrared spectra of raw materials and product (Fig.22) shows disappearing absorption bands of planar CO_3^{2-} anion with D_3h symmetry[6] [183,186,372-374] including strong band of antisymmetric stretching at 1465 cm^{-1} ν_3, weak band of symmetric stretching at 1072 cm^{-1} ν_1, out of plane bending at 856 cm^{-1} ν_2 and antisymmetric bending vibration at 702 cm^{-1} (ν_4). There are also three combination bands $2\nu_1+\nu_2$, $\nu_1+\nu_4$ and $\nu_1+\nu_4$. Corundum in raw mixture shows four main absorption bands of stretching of (AlO_6) octahedra at 639, 591, 489 and 448 cm^{-1} [375,376].

On the contrary, the $SrAl_2O_4$ structure is built up from (AlO_4) tetrahedra with the T_d symmetry and the structural lattice channels are occupied by Sr^{2+} ions [377]. The bands appearing in the spectral regions from 900 to 780 cm^{-1} and from 650 to 550 cm^{-1} belong to antisymmetric and symmetric stretching of (AlO_4) tetrahedra. The bands related to the doublet of bending of O-Al-O are located at 446 and 418 cm^{-1}.

Simultaneous TG-DTA (a) and EGA (b) analyses of the mixture of strontium carbonate and alumina (Fig.23) show sharp exothermic peak at the temperature of 967 °C, which divides the huge endothermic effect of thermal decomposition of strontium carbonate occurring within the temperature range from 810 to 1020 °C. The CO_2 bands appear on EGA. That means, that

---

6 The D_3h symmetry of CO_3^{2-} anion is reduced to C_s for carbonates from group of aragonite. It leads to the splitting of degenerated modes ν_2 and ν_4 and amount of vibration modes in infrared spectrum is increasing. Furthermore, the intensity of fully symmetric stretching mode ν_1 is increasing (this mod is not IR active for carbonates from the group of calcite).
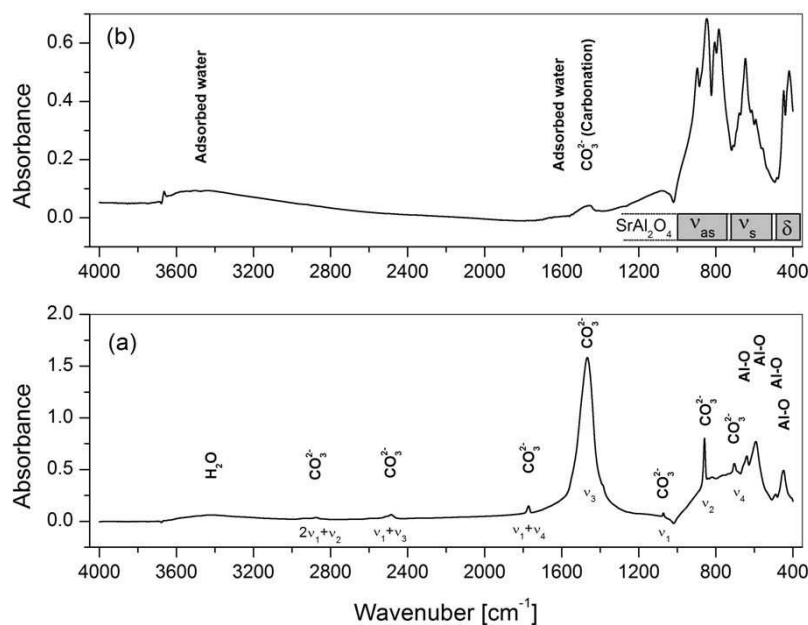
Figure 22. Initial (a) and final infrared spectra (b) of strontium aluminate clinker.

formed $SrAl_2O_4$ phase covered the surface of decomposed $SrCO_3$ particle and this layer slowed down the diffusion of CO_2 from the reaction interface to disappearing $SrCO_3$ core. Therefore, the thermal decomposition of $SrCO_3$ was suppressed. The volume changes caused by the decarbonation and recrystallization of products led to the formation of cracks, which enabled easy diffusion of CO_2 through the layer of the product. The mass of the sample was reduced by 17.7 wt. % during this process.
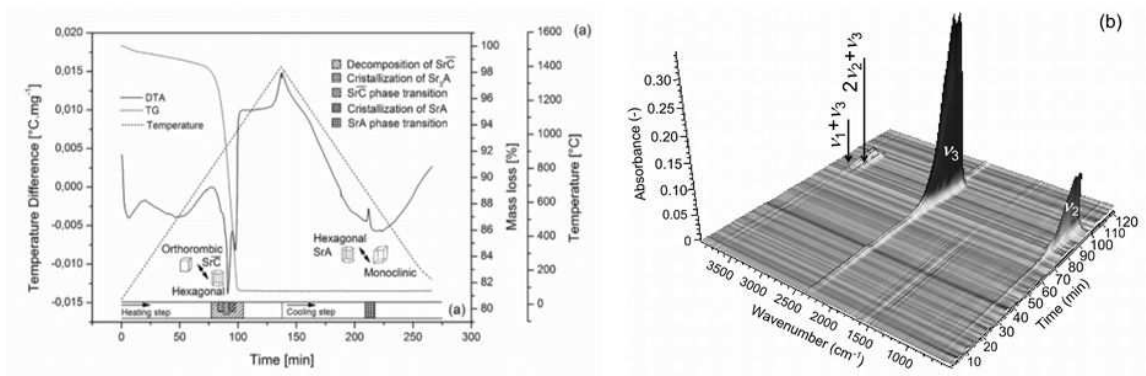
Figure 23. Thermal analysis of strontium aluminate clinker: simultaneous TG-DTA (a) and EGA (b) assessment using the heating rate of 10 °C min⁻¹.

The reaction interface (Fig.24) abundance of SrO (outer side of formed strontium aluminate layer) or Al_2O_3 (inner side) component led to the formation of tri-strontium aluminate (Sr_3A) and strontium hexaaluminate (SrA_6). The equilibrium composition of strontium aluminate (SrA) was then established via the opposite direction diffusion of Sr^{2+} and Al^{3+} ions. The opposite

model, i.e. Al_2O_3 particle surrounded by $SrCO_3$, where the formation of strontium aluminate is limited by the diffusion of Sr^{2+}ions into the disappearing alumina core cannot explain the observed behaviour. Therefore, formed Sr_3A is actually the mesophase during the process of reaction [378].
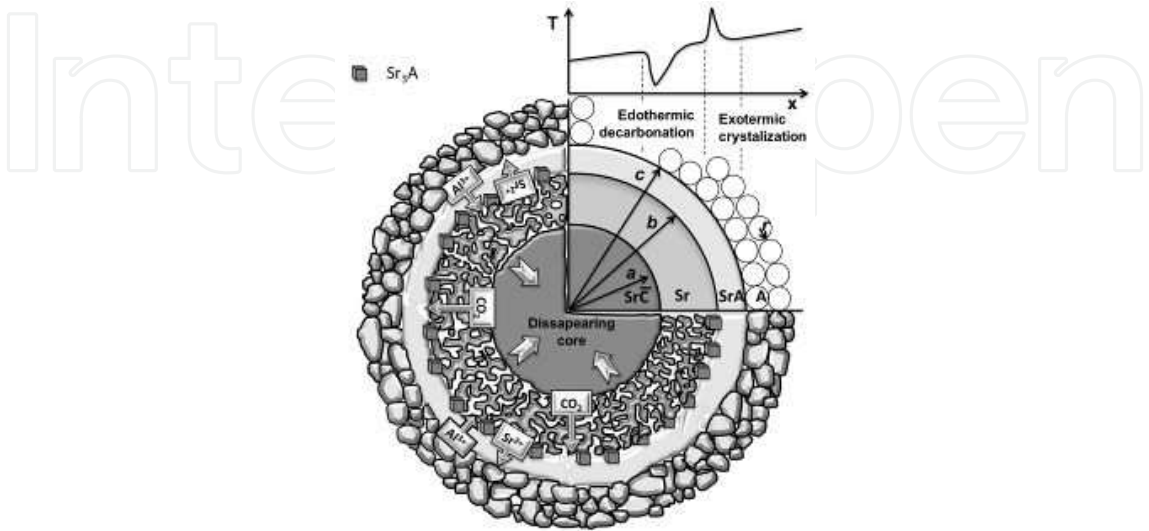

Figure 24. Mechanism of formation of strontium aluminate [379].

The cooling zone in (Fig.23) showed an exothermic effect of reversible transformation of hexagonal high-temperature modification of $SrAl_2O_4$ to low-temperature monoclinic phase at the temperature of 650 °C. During repeated cycle of heating, the exothermic transformation took place at higher temperature. The temperature hysteresis of this transformation increased linearly with the heating rate (Fig.25). Therefore, the limit value of 9.10 ± 0.07 °C should be estimated from the linear fit for $\Theta \to 0$ [379].
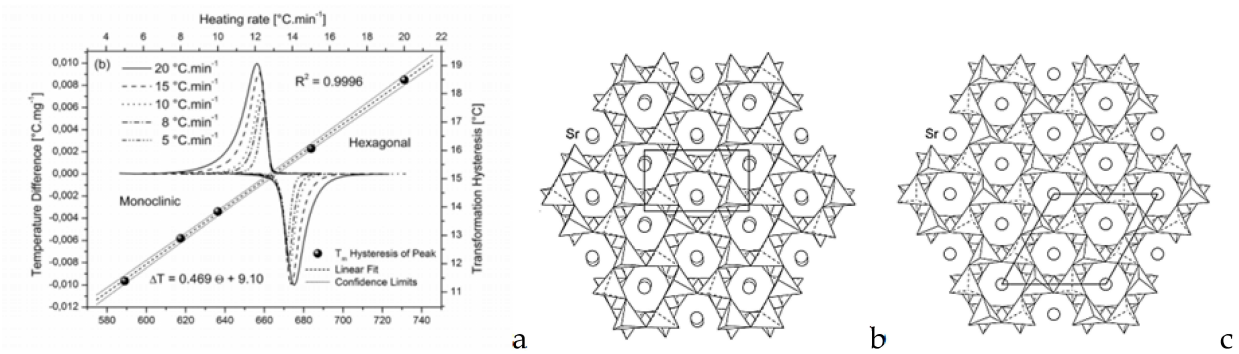

Figure 25. Temperature hysteresis in the polymorphic transformation (a) [379] between monoclinic (b) and hexgonal strontium aluminate (c) [24].

The recorded XPS (X-ray photoelectron spectroscopy) spectrum of strontium (Sr3d) in prepared strontium aluminate cement is presented in Fig.26. The results indicate that the

structure of $SrAl_2O_4$ includes two binding states of strontium in the structure of strontium aluminate distributed in the ratio close to 1:2, similarly as was described for the structure $CaAl_2O_4$ where two Ca(I) and Ca(II) had octaedric coordination while Ca(III) was coordinated by six O^{2-}ions in the trigonal antiprism [380].
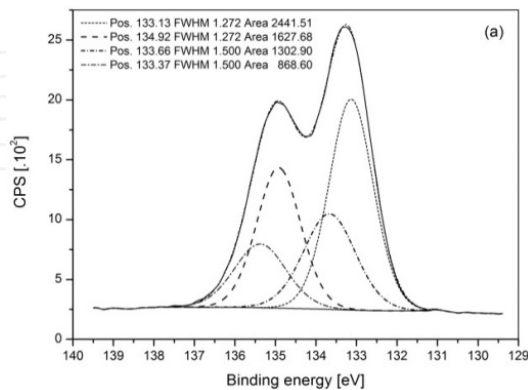
Figure 26. XPS spectrum of strontium from prepared strontium aluminate clinker.

3.2. Kinetic of formation of strontium aluminate

The Kissinger plot related to the kinetics of strontium aluminate and tri-strontium aluminate phase formed from the mixture of raw materials is shown in Fig.27.
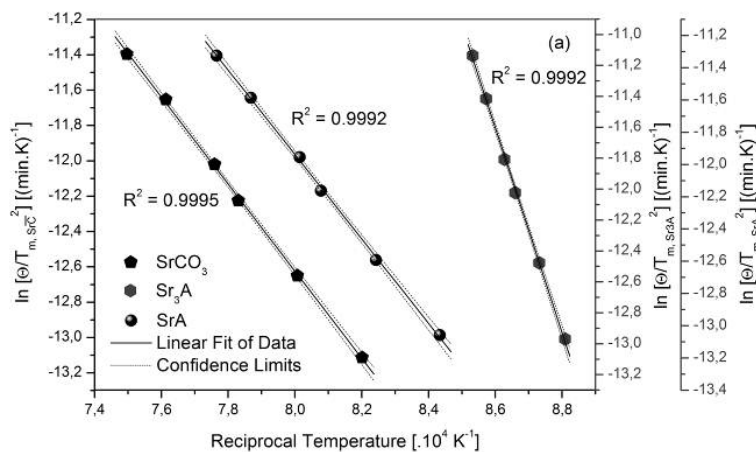

Figure 27. Kissinger plot related to the formation of SrA and Sr_3A clinker phase [379].

The apparent activation energy and the frequency factor relating to the formation of Sr_3A are 551 kJ mol^{-1} and 1.69 10^{23} s^{-1}, respectively. The value of kinetic exponents calculated according to Eq.113 in Chapter 1 is 4.0, hence the process is driven by constant nucleation rate of a new phase. SrA shows the activation energy and the frequency factor of 218 kJ·mol^{-1} and 1.63 10^7 s^{-1}, respectively. The value of kinetic exponent is equal to 5.2. Therefore, the crystallization of SrA phase is driven by increasing nucleation rate of a new phase [379].

3.3. Sintering of strontium aluminate clinker

Heating microscopy (Fig.28) showed the expansion of specimen up to 113 % of its original height. For the temperatures higher than 1050 °C the growth of specimen decreased. The initial temperatures of solid-state and liquid state sintering were determined to be 1450 and 1550 °C, respectively.
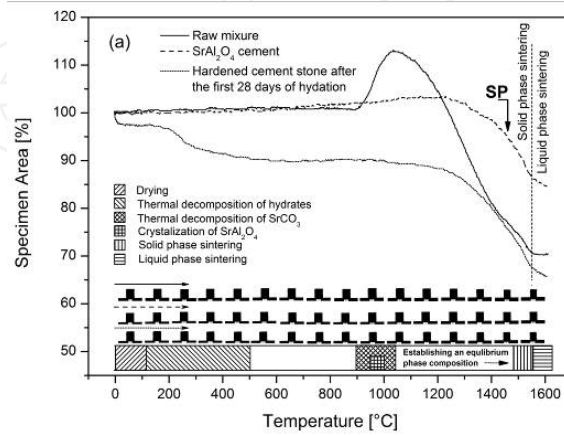
Figure 28. Behaviour of raw material specimen during heating with the heating rate of 5 °C min⁻¹ [379].

The information on the mechanism and kinetics of the processes occurring during the synthesis of strontium aluminate clinker were used for the calculation of correct conditions (Fig.29) during the thermal treatment from kinetic triplet, i.e. activation energy, frequency factor and kinetic factor (Chapter 4.3.2).
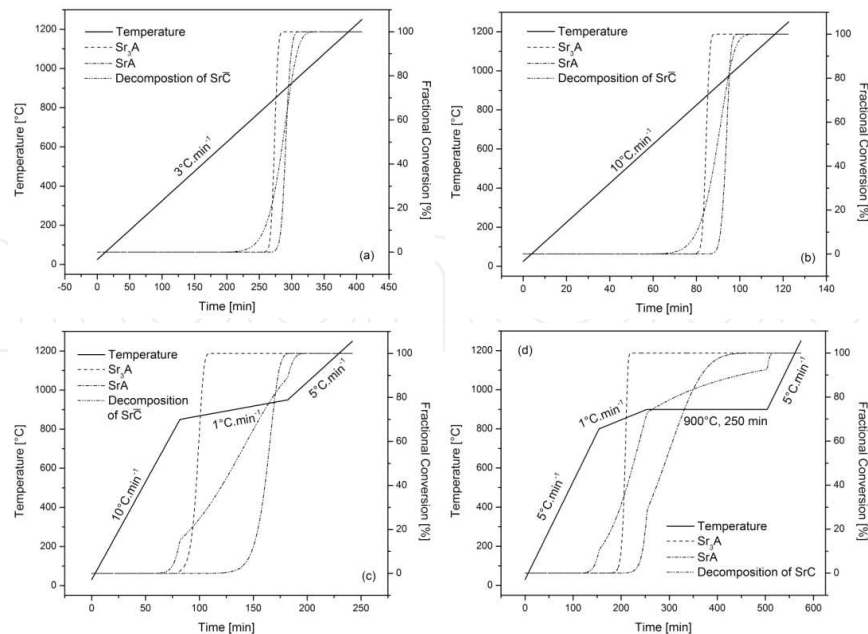
Figure 29. Formation of strontium aluminate using single ramp (a), fast ramp (b), slow heating upon reaction zone (c) and isothermal condition in reaction zone (d).

4. The influence of degree of saturation

The influence of saturation degree (*SD*, Eq.36 in Chapter 2) on the equilibrium composition of the product during the thermal treatment of strontium aluminate raw mixture consisting of $SrCO_3$ and Al_2O_3 is shown in Fig.30. Lower values of saturation of raw materials by strontium oxide support the formation of strontium dialuminate[7] while the amount of tri-strontium aluminate and strontium oxide increases with increasing SD_{SrO}. These phases significantly contribute to the heat release during mixing the clinker with water. In order to avoid the danger of overheating of mixture, the saturation degree ≥ 100 % shouldn't be used. The theoretical value, which was estimated as the highest allowed value of saturation degree for which the equilibrium amount of SrO is inconsiderable is close to 95 %.
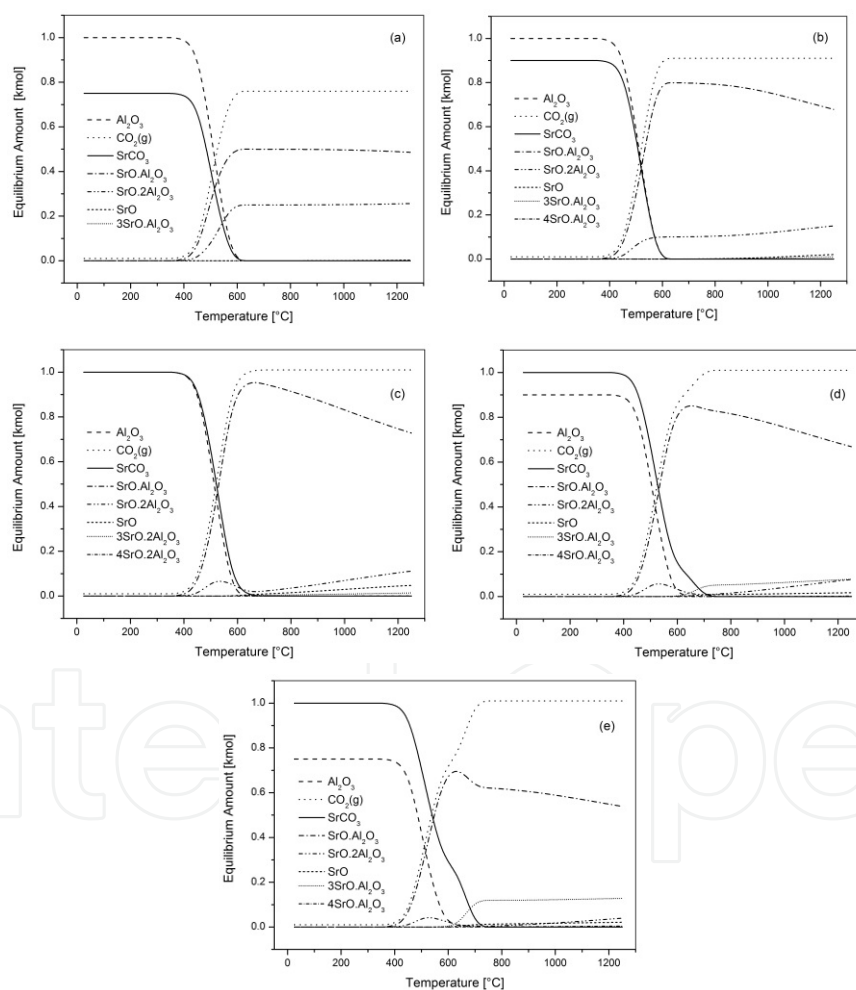

Figure 30. Influence of SD_{SrO} on the calculated equilibrium composition of reaction products: 73.8% (a), 88.6 (b), 98.4 (c), 109.4 (d) and 131.2 (e).

---

7 Formation SrA_6 is preferred from the formation of SrA_2 during thermal treatment of raw meal (please see discussion in Chapter 1.5).

5. Final treatment of strontium aluminate cement

Grinding and fine milling of strontium aluminate clinker (Fig.31) prepared via the calcination of pellets (a) or fine raw material powder (b) provided cement with the median of particle size of 7.52 μm (Fig.33), which was used for the hydration experiments described in the next chapter as well as for other applications described in Chapters 6-8. Using pressed pellets may influence the behaviour of raw material during the thermal treatment as was already discussed in Chapter 2.8.
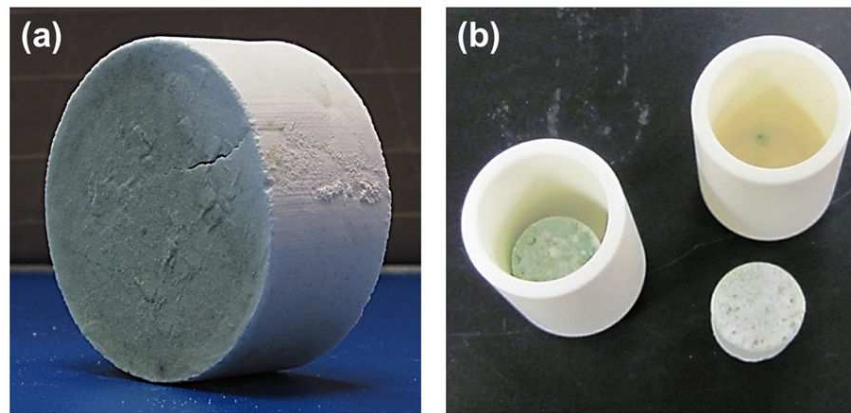
Figure 31. Strontium aluminate clinker prepared from pelletized (a) and fine powdered (b) mixture of raw materials.

The SEM picture of strontium aluminate cement (Fig.32) shows larger subhedral particles with some glass-like faces surrounded by aggregates consisting of closely associated smaller particles.
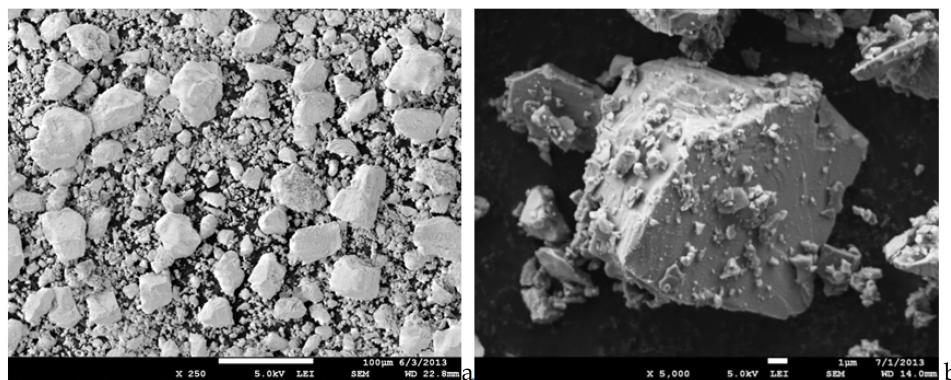
Figure 32. SEM picture of fine ground strontium aluminate cement.

The particle-size distribution (PSD) and the cumulative distribution function of prepared binder are shown in Fig.33. The multimodal particle size distribution in ground clinker should be explained by the content of other phases of different grindability (Fig.21) and of glassy phase.
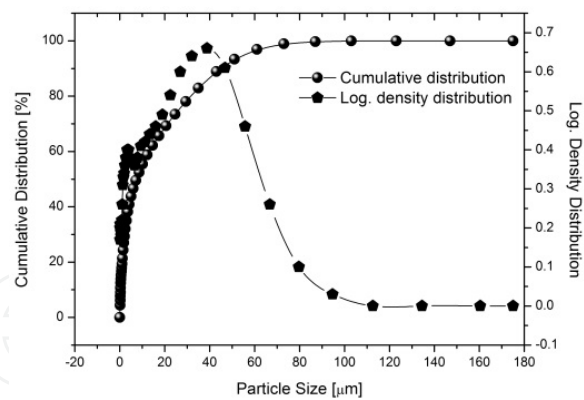
Figure 33. Particle size distribution of strontium aluminate clinker [379].

6. Clinker quality evaluation

The specific surface, the particle size distribution (Chapter 3.5 and Chapter 6.1.2), the content of major and minor clinker phases (Chapter 2.5) in cement are the main parameters which can be used for the evaluation of quality of strontium aluminate clinker similarly to other binders such as AC and PC. These parameters define the proportion of fine and coarse particles in cement. This proportion controls the water demand, the setting and hydration reactions [381-385].
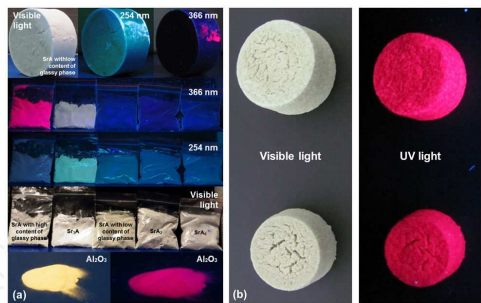

Figure 34. The clinker phase (Sr_3A, SrA, SrA_2 and SrA_6) and alumina (a) and strontium aluminate clinker with high content of glassy phase (b) under visible and UV light.

Therefore, low firing temperature or rough milling procedure can be used in order to reduce initial high reactivity of SrA cement with water. The phosphorescence of calcinate can be applied to evaluate the firing process (estimate the amount of unrecated alumina, Fig.34). Furthermore, the phosphorescence under UV light can be used for marking of cement or for preparation of cement layer or concretes of special properties.